Lift Reduction by Counter Flowing Wall Jets

Nader H. Al-Battal[1], David J. Cleaver[2] and Ismet Gursul[3]

Department of Mechanical Engineering, University of Bath, Bath, BA2 7AY, UK

Counter flowing wall jets are proposed to reduce extreme loads, enabling lighter and more efficient aircraft. Upstream blowing on the upper surface of a NACA0012 airfoil at a Reynolds number of 660,000 was investigated by means of force, pressure and particle image velocimetry measurements, and was found to be more effective than blowing normal to the surface. Blowing locations near the trailing edge are more effective for low angles of attack; locations near the leading edge are more effective for higher angles of attack. At the stall angle of attack, a maximum reduction in the lift coefficient was observed as ΔC_L = -0.33 when the blowing location was at x_J/c = 0.08 for the largest flow rate coefficient (C_Q = 0.44%) tested. Even for completely separated flows, upstream blowing near the trailing-edge can modify the recirculation region and cause the shear layer to deflect upwards, resulting in a reduction of lift. This is a significant advantage over mechanical flaps placed near the trailing-edge, which remain in the separated flow and lose their effectiveness.

Nomenclature

α = angle of attack

C_μ = momentum coefficient

C_L = lift coefficient

C_p = pressure coefficient

C_Q = volumetric flow rate coefficient

ΔC_L = change in lift coefficient relative to baseline

c = chord length

[1] Postgraduate Student, Department of Mechanical Engineering, Student Member AIAA.
[2] Lecturer, Department of Mechanical Engineering, Member AIAA.
[3] Professor, Department of Mechanical Engineering, Associate Fellow AIAA.

h_J = slot width

s = span

ρ_J = density of jet

ρ_∞ = density of freestream flow

x_J = location of jet

U_J = jet velocity

U_∞ = freestream velocity

Re = Reynolds number

I. Introduction

Gusts are often the critical load cases for civil transport aircraft and therefore determine the mass of the structure. In addition, gusts are also detrimental to passenger comfort. Gust encounters therefore significantly impact the efficiency and performance of the aircraft. Therefore, gust load alleviation has become an important aspect [1]. Current technology comprises of ailerons and spoilers. These control surfaces are sized for manoeuvres and therefore become ineffective at high gust frequency due to their large inertia. Numerical studies performed by Moulin and Karpel [2] have also indicated that current aileron designs have a decreasing effectiveness with increasing flight velocity. Therefore, highly responsive actuators are essential for gust load mitigation. The ultimate use of these actuators would be in the form of finite-span wall-jets located outboard sections of a 3D wing in order to reduce the sectional lift and bending moment.

Small mechanical devices near the trailing-edge [3,4] were proposed. Low inertia mechanical actuators, such as mini-tabs placed perpendicularly to the airfoil upper surface [4,5], were considered for the mitigation of aerodynamic loads. Heathcote *et al*. [5] investigated the effect of mini-tab location, up to near the leading-edge, and observed significant influence on the magnitude of lift reduction and the lift curve gradient as a function of angle of attack. Placement of the mini-tab near the mid-chord provided more uniform lift reduction across a wider range of angle of attack. On the other hand, placement of the mini-tab near the leading-edge provides the largest lift reduction with increasing angle of attack. As the location of the mini-tab is varied from the leading-edge to the trailing-edge, the flow over the upper surface of the airfoil varies from the fully separated one to the fully attached one that is deflected at the trailing-edge (similar to a Gurney flap).

Fluidic actuators that use jet blowing perpendicular to the airfoil upper surface near the trailing-edge were proposed [4,6]. Figure 1 illustrates the concept of "normal blowing" for the aircraft wings. This can be considered to be similar to conventional jet-flaps [7], which have been used to increase the lift, although the desired outcome is the opposite (lift decrease versus increase). The jet strength is often defined using a non-dimensional parameter, momentum coefficient C_μ, which in the two-dimensional case becomes:

$$C_\mu = \frac{\rho_J h_J U_J^2}{\frac{1}{2}\rho U_\infty^2 c}$$

Studies of jet-flaps focussed on large momentum coefficients of the jet in order to produce high lift. However, for flow control applications, much smaller momentum coefficients (typically C_μ=0.01-0.03) were considered, whether the lift increase or decrease was the objective [4,6,8]. As the momentum coefficients are typically small, the contribution of the momentum of the jet blowing perpendicular to the airfoil surface (reaction force) to the total lift coefficient is small (on the order of 10^{-2}). Yet it was shown that a change of lift coefficient $\Delta C_L \approx 0.15$ can be obtained for a momentum coefficient of C_μ= 0.03, hence an effectiveness of $\Delta C_L/C_\mu \approx 5$ has been achieved [8].

Blowing perpendicular to the airfoil surface might not be the most effective blowing direction, if the purpose is to deflect the flow near the trailing-edge region. For typical momentum coefficients used for flow control (on the order of 10^{-2}) and blowing slot width ratio h_J/c (on the order of 10^{-2}), the magnitude of the jet velocity is on the order of the freestream velocity. Hence, for the jet velocity ratio around unity, sufficient deflection of the flow may not be achievable. If the jets in crossflow [9] are considered to find a rough estimate, the jet trajectory (defined as the time-averaged streamline originating at the jet exit) reaches an asymptotic distance of 2 to 4 jet exit width h_J from the wall for U_J/U_∞ = 1 to 2. In contrast, counter flowing wall jets can provide larger deflections (see the sketch in Figure 1). The time-averaged dividing streamline (originating from the stagnation point on the wall) can reach an asymptotic distance of 7 to 15 jet exit width h_J from the wall [10] for U_J/U_∞ = 1 to 2. Kinematic analysis of such flows via the free-streamline theory was attempted in [11], which suggested that the only parameter is the jet velocity ratio U_J/U_∞. It has been found that the counter flowing wall jets introduced by plasma actuators placed on the lower surface of the airfoil near the trailing-edge can create the virtual Gurney flap effect [12].

Potential application of counter flowing wall jets, called as “upstream blowing” in this paper, in comparison to “normal blowing” is sketched in Figure 1.

Blowing at upstream locations might be more advantageous as suggested by the experiments with mini-tabs [5]. Counter flowing wall jets can be more effective on the upper surface when the adverse pressure gradient becomes stronger with increasing angle of attack. In this paper the effectiveness of the counter flowing wall jets placed on various chordwise locations of the airfoil upper surface is investigated in terms of the lift reduction capability and compared with the normal blowing. Force measurements are performed over a range of angles of attack and jet velocity ratios. Particle Image Velocimetry (PIV) measurements are undertaken for angles of attack of interest, to further enhance the understanding of flow physics associated with the jet blowing. Pressure measurements are performed for the same cases as those selected for PIV, in order to observe the effect on the pressure along on the airfoil surface. The ultimate goal is to develop new actuators that can operate at frequencies beyond the range of conventional load control devices. This study is the first step, before we look at the unsteady actuation.

II. Experimental Techniques

Experiments were performed in a low-speed closed-circuit wind tunnel at the University of Bath. The working section of the wind tunnel has a length of 2.77 m, height of 1.51 m and width of 2.12 m. Turbulence intensity of the wind tunnel was determined as less than 0.5% at U_∞ = 20 ms^{-1}. The freestream velocity for the experiments performed was U_∞ = 20 ms^{-1}, which equates to a Reynolds number of *Re* = 660,000. Given that load alleviation concept is the same in different applications, including UAVs, rotorcraft and wind turbines, we have decided to test a generic airfoil. The symmetrical NACA 0012 airfoil was selected due to the large database of aerodynamic data for the profile. The chord length was c = 500 mm and span was b = 1500 mm. The wing therefore had a 5 mm (1% of the chord length) clearance between the wind tunnel walls so as to prevent tip effects and simulate an infinite-span wing or airfoil. To instigate boundary layer transition to turbulence, trip wires of 0.3 mm diameter were fixed at x/c = 0.1 on the upper and lower surface of the airfoil. This location coincides with the point of maximum surface velocity, which has been suggested as an effective position for NACA four-digit airfoils [13]. The angle of attack was varied in the range of α = 0° to 20°. Jet blowing slots with a width of h_j = 1 mm were placed at five chord-wise locations x_J/c = 0.08, 0.60, 0.75, 0.85 and 0.95.

The first 0.725c of the airfoil was composed of a carbon fibre composite, reinforced with an internal aluminum alloy structure and Rohacell® XT foam for stiffness and retaining low weight, see Fig. 2. Two aluminum tubes with square cross-section were installed as plenum chambers at x/c = 0.08 and 0.60. These tubes had a length and width of 1.5 m and 0.022 m, and fed air to the corresponding slots at these chordwise loactions. The remaining 0.275c of the airfoil was rapid prototyped using DuraForm® PA plastic due to its complex internal design caused by more densely placed blowing slots. The SLS method produces a surface tolerance of 0.1 mm. This was finished through repeated cycles of paint and sanding with extremely fine emery paper to give a perfectly smooth, almost reflective finish, without changing the airfoil profile. The material used for the trailing edge has a tensile strength of 4000 MPa and produces negligible deformation when subjected to the internal pressures and external freestream pressures experienced at these very low speeds (20 m/s in our case). This trailing-edge section was manufactured in five interchangeable parts. It is designed to act as a plenum chamber for blowing slots located downstream of x/c = 0.725. The slots extended the entire span so as to create a quasi-two-dimensional blowing. To ensure the jet flow was evenly distributed along the span, porous polyethylene sheets of 2 mm thickness were installed beneath the jet exit, encouraging a more uniform distribution. This uniformity was measured using a hot-wire probe to always be greater than 90%.

Normal blowing was achieved by cutting slots perpendicular to the surface. However, for upstream blowing to be performed, an additional carbon fiber piece was attached, as shown in Fig. 2a. The piece with a thickness of 0.28 mm (0.056%c) extends 5 mm (1%c) upstream of the jet, and protrudes above the wall by 0.5 mm (0.1%c). The jet exit width, which creates an unavoidable step on the airfoil surface, was kept minimal at h_j = 0.5 mm. To ensure that the protruded step did not significantly alter the lift force, additional baseline (no-blowing) force measurements were performed for each location of the upstream blowing slot, as will be shown later. The piece induced a negligible change in lift force at all angles of attack considered. Throughout this study, unused slots were taped over to prevent unwanted transition points.

The flow rate was controlled through a manual valve and was measured using an SMC Digital Flow Switch PF2A703H-F10-68. This has a stated repeatability accuracy of ± 1%. During experiments, fluctuations in volumetric flow rate readings were observed to be limited to ± 2%. Such errors lead to an overall uncertainty of 2.2%. The flow meter was calibrated to determine the flow rates. However, the jet velocity profile was measured by a hot-wire anemometer to calculate

the blowing strength more accurately. Two dimensionless parameters for blowing are considered: the momentum coefficient C_μ and the volumetric flow rate coefficient, defined as:

$$C_Q = \frac{h_J U_J}{U_\infty c}$$

The two parameters are related as $C_\mu = 2C_Q^2/(h_J/c)$, however we believe that C_Q is more meaningful. First of all, the theoretical modelling of the counter flowing wall jets [11] suggests that the main parameter is U_J/U_∞. Secondly, unlike the applications in which the momentum addition is important (such as the delay of flow separation), forced separation of an attached boundary layer can be considered due to a source whose strength is proportional to C_Q. A similar situation occurs for the cases where the suction acts as a sink [14,15] and the volumetric flow rate coefficient becomes the main parameter. In addition, this parameter is representative of the power input into the system. In our experiments, C_Q was varied in the range of 0.20% to 0.44%, which corresponds to the C_μ range of 0.4% to 2% (normal blowing, h_j = 1 mm) and 0.8% to 4% (upstream blowing, h_j = 0.5 mm) when the jet velocity ratio is varied. Local definitions of the momentum coefficient and volumetric flow rate coefficient based on the local velocity may be more appropriate, however this is not practical as a global parameter.

A. Hot-Wire Measurements

Hot-wire measurements were taken to determine the jet velocity in absence of the freestream, using a TSI® 1210 – T1.5 hot-wire anemometer connected to a DISA 56C16 General Purpose Bridge. A constant temperature anemometer bridge card was tuned specifically to the hot wire. A 12-bit analogue to digital converter amplified the output signal from the General Purpose Bridge for analysis. Calibration of the hot-wire anemometer was performed by placing the hot-wire probe and a calibrated Pitot tube within a pipe. A Digitron 2020P digital manometer was connected to the Pitot tube to record dynamic pressure readings. These readings were used to determine the velocities at which hot-wire measurements were taken. A total of 42 hot-wire measurements were taken within a velocity range of 0 – 50 ms^{-1}. Voltage readings were then approximated in to a non-linear equation, in the form of King's Law equation. Hot-wire measurements were performed for each jet location, at 59 equally distributed spanwise positions. With a sampling frequency of 2

kHz, 20,000 samples were taken. The measurements confirmed spanwise uniformity greater than 90% for all slots.

B. Force Measurements

The airfoil was mounted below a two-component aluminum binocular strain gauge force balance, which was manufactured in-house, similarly to previous experiments carried out at the University of Bath [16,17]. Strain gauges were attached to the force balance at the points of maximum strain, and configured in a Wheatstone bridge circuit. The voltage signals from the strain gauges were amplified and conditioned using a 12-bit analogue to digital converter. Output signals were collected using LABVIEW® 7.1, with a sampling rate of 2 kHz for 20,000 samples. In order to minimize uncertainty, measurements were repeated six times for each angle of attack considered. Due to the force balance rotating with angle of attack, output voltages were post-processed in MATLAB® in order to obtain corrected forces relative to the direction of the freestream velocity.

Calibration of the force balance was performed before each group of experiments to mitigate inaccuracies. Calibration curves of the normal force-to-voltage were obtained by applying known weights to a thin cable fixed at the mid-span of the wing, through a low friction pulley system. Distinct intervals of 16 calibration points were collected for forces ranging between 0 to 150 N. Force measurements were performed for angles of attack between $0° \leq \alpha \leq 20°$ in one degree intervals. Uncertainty analysis, with the methods of Moffat [18], determined the uncertainty of the dynamic pressure q measurements within the wind tunnel to be 1.6%. Uncertainties in force coefficient were typically 2.6% for pre-stall angles of attack. The uncertainty in angle of attack was 0.25°.

Although both lift and drag measurements were taken, only the lift data will be discussed in this paper. As the ultimate goal of this research is to develop high-frequency fluidic actuators for lift reduction, the effect on the lift is the primary concern. Even though the drag increases when the actuator on the upper surface is activated, such a short-duration drag increase is not a major concern compared to the main objective of lift reduction.

C. Pressure Measurements

Pressure measurements were performed with 40 pressure taps located at the mid-span of the airfoil. Taps of two millimeter diameter are located on both the upper and lower surfaces. The jet slots interfere with positioning on the upper surface giving 19 pressure taps located on the upper surface and 21 taps on the lower surface. Pressure measurements were performed using a Scanivalve Corp PDCR23 differential pressure transducer with a range of ±6900 Pa. The pressure transducer was calibrated using a Druck DPI portable transducer calibrator. To minimize uncertainty, each use consists of three repeats sampled at 1 kHz. Typical uncertainty with the time averaged pressure measurements is estimated to be 2.1%.

D. Particle Image Velocimetry Measurements

A 2D-PIV system was used to measure the flow field of the upper surface at z/b = 0.6. An EverGreen 200mJ 15Hz Nd:YAG double-pulse dual laser, positioned outside of the wind tunnel, see Fig. 2b, illuminated atomized olive oil droplets with a mean size of 1 µm. This size is suitable according to the Stokes drag equation [19]. Two TSI® PowerView™ CCD 8 MP cameras (3,312 x 2488 pixels) in a tandem configuration were positioned at a distance of 1200 mm underneath the plane of interest. The cameras were fitted with two Nikon AF 50 mm NIKKOR f/1.8D lenses. The dual camera arrangement was configured to have an overlap region of 35 mm. A MATLAB code is used to combine the two images together on to a grid, while using a weighted average for the overlap region. This involves averaging vectors of the two images within this region, with a bias towards the image nearest to the middle of the region. As such, both images hold an equal weight at the centre of the region. The cameras and laser were synchronized with the TSI® LaserPulse 610034 synchronizer. Separately, close-up images were taken with one TSI® PowerView™ CCD 2 MP camera fitted with a Nikon 200 mm f/4 AF-D Macro lens.

The PIV images were analyzed using a recursive fast Fourier Transform cross-correlator with the TSI® Insight 3G software. Interrogation window sizes for the entire airfoil surface and close-up images were of 32 x 32 pixels and 40 x 40 pixels, respectively. This produced a spatial resolution of 4 mm (0.8%c) for images of the entire airfoil surface and 1.3 mm (0.26%c) for the close-up images. The time-averaged velocity field data were generated from 450 image pairs. Vector fields from images pairs were merged together with further post-processing using MATLAB®. The custom made MATLAB® code utilized a weighted average to accurately merge

the overlap region. Error involved with laser alignment is estimated to be 1 mm. The error associated with the calibration scale is estimated to be 0.2% of the chord length. Uncertainty in velocity measurements were typically 3%.

III. Results and Discussion

A. Baseline Airfoil

Figure 3 shows the variation of the lift coefficient for the no-blowing case against similar measurements from the literature. The measurements of Sheldahl and Kilmas [20], and Jacobs and Sherman [21] were performed at Reynolds numbers of Re = 7 x 10^5 and 6.6 x 10^5, respectively. The linear region of the current measurements is in good agreement, in particular to Jacobs & Sherman. There is wide variation in the post-stall region across the data sets. However, the agreement between the current data and Jacobs and Sherman [21] is pretty good. As discussed previously, upstream blowing was created by applying an auxiliary piece that diverts flow tangentially upstream along the upper surface (see Fig. 1). Therefore, it was important to ensure that this slight protrusion did not significantly affect the lift generated by the baseline airfoil. As shown in Fig. 3, additional force measurements for zero jet velocity with the piece attached were performed at jet locations x_J/c = 0.08, 0.60 and 0.95. It can be confirmed the addition had a negligible effect on the lift force generated across all angles of attack and jet locations.

B. Upstream versus Normal Blowing

Figure 4a shows the change in the lift coefficient as a function of momentum coefficient for α = 0°. Because of the symmetry of the baseline airfoil at zero angle of attack, we compare our results of lift reduction for normal and upstream blowing with those of lift increase from the literature [8,22-24]. These cases of lift increase (jet placed on the lower surface and near the trailing-edge) are shown with open symbols. As Spence [7] proposed that the change in lift coefficient is proportional to the square-root of the momentum coefficient, we also present a curve fit of the same form, shown with the solid line. Although there is a large scatter of the data from the literature, our data (shown with solid black symbols) for x_J/c = 0.95 show the same trend with the curve fit and also show good agreement with Traub et al. [8] data. The Traub *et al*. data (normal blowing location *x/c*=0.98) are shown with open square symbols. The closest location that we have is *x/c* = 0.95 for which the data are shown with black filled square symbols. There is a very good

agreement between the two data sets. We also note that both normal blowing and upstream blowing give similar results for x_J/c = 0.95. For the other jet locations, which are all upstream, the magnitude of the lift reduction clearly decreases. There is monotonic reduction of the change of the lift as the blowing location approaches the leading-edge for both normal and upstream blowing. Figure 4b shows the change in the lift coefficient as a function of momentum coefficient for α = 13°. For the same momentum coefficient, the upstream blowing (solid circles) provides much larger lift reduction than the normal blowing (solid squares) for all blowing locations. Also, unlike the zero angle of attack case, blowing at upstream locations seems preferable.

Now we return to our earlier discussion of the two parameters C_μ and C_Q. If Figure 4a and 4b were plotted as a function of C_Q rather than C_μ, both normal and upstream blowing flow rate coefficient values would span the same range. However, the lift reduction data do not collapse with neither C_μ nor C_Q. The purpose of blowing, in this paper, is not to inject momentum to the flow, but to stagnate the local flow in order to modify the effective camber of the airfoil. Allowing the jet to act as a source suggests a source coefficient in the form of volumetric flow rate coefficient. Nevertheless, we shall continue to report both parameters.

Time-averaged force measurements shown in Fig. 5, compare upstream and normal blowing as a function of angle of attack at the maximum volumetric flow rate coefficient ($C_Q = 0.44\%$). Normal blowing at x_J/c = 0.08, shown in Fig. 5a, has a negligible change on lift coefficient until α = 5°, and then causes an increase by an average of ΔC_L = 0.06 until α = 11°. Hence, normal blowing provides negligible lift mitigation when located near the leading edge. In contrast, efficiency of lift mitigation with upstream blowing appears to be dependent on angle of attack. At low angles the effect is negligible or small, but increases with increasing angle of attack, reaching a peak at the stall angle α = 13°, of 30% reduction. Alleviation of lift is seen to extend into the post stall region, with the point of stall being delayed to α = 19°. Unlike normal blowing, upstream blowing appears to provide effective manipulation of the separated shear layer near the leading-edge.

As the jet location moves to x_J/c = 0.60, shown in Fig. 5b, upstream blowing exhibits similar behavior at high angles of attack, to the jet at x_J/c = 0.08 but the effect is weakened. It is able to alleviate lift at all angles considered. In particular, near the stall angle, the effectiveness of the

upstream blowing at x_J/c = 0.60 to manipulate the massively separated shear layer is impressive. However, the normal blowing jet is rendered ineffective for all angles of attack.

Normal blowing appears to work effectively when located near the trailing edge, as shown in Fig. 5c. At x_J/c = 0.95, it is able to attain an approximately constant change in lift coefficient of ΔC_L = -0.15 up to stall. This reduction in lift is augmented with upstream blowing by approximately 33%. In addition, upstream blowing continues to have an influence on the lift generated at high incidences. This is even more interesting near the stall angle, considering that upstream blowing near the trailing-edge has an influence on the separated flow originating from near the leading-edge. With both methods being tested with the same volumetric flow coefficient, it is clear that upstream blowing is more effective across the board and is the preferred method for lift mitigation.

Time-averaged velocity flow fields are presented in Fig. 6 to compare measurements for the baseline case, normal blowing and upstream blowing at x_J/c = 0.95, for the maximum flow coefficient of C_Q = 0.44%. These flow fields correspond to the force measurements shown in Fig. 5c. At α = 0°, blowing produces deflection in streamlines near the location of the jet. However, differences between blowing directions are not discernible in the global flow field. Hence, the region of interest near the trailing edge is analyzed with smaller grid size in the inset, where the location of the blowing is also shown. The baseline airfoil exhibits attached flow along the entire upper surface. However, normal blowing generates a separation region which extends from the jet location to the trailing edge. The small separation region not only deflects the streamlines above, but also deflects the flow from the lower surface upwards. These creates a virtual change in the direction of the flow near the trailing-edge, which otherwise would be parallel for α = 0°. With blowing near the trailing-edge, the effect is similar to that of a Gurney flap, which creates a similar separation region. Similar flow field behavior for a normal jet flap at x_J/c = 0.95 with α = 0° but on the lower surface has been observed by Blaylock et al. [4]. Due to this separated region, the streamlines external to it are deflected upwards, causing an upwash effect. The normal jet is capable of deflecting the flow from the lower surface, particularly when located near the trailing edge. Due to such close proximity to the lower surface, the normal jet is able to modify the Kutta condition to a greater effect, and hence the circulation of the airfoil as argued by [4]. For upstream blowing the point of separation occurs outside the region of interest of the inset, indicating a larger separated region is formed in comparison to normal blowing. Therefore, the larger region of influence produced by upstream blowing is able to affect the upper surface pressure gradient and

modify the camber to a greater extent. This effect contributes to understanding the difference observed in force measurements; upstream blowing jet reduces lift by $\Delta C_L \approx$ -0.06 more than normal blowing.

Increasing the angle of attack to α = 5°, increases velocity magnitude near the leading edge. When employing either of the two blowing methods, a reduction in this velocity magnitude is observed, implying a reduction in suction. Normal and upstream blowing maintain ability to modify the effective camber of the airfoil, as flow continues to be diverted away from the surface of the airfoil, as seen in Fig. 6. The change in lift coefficient for normal blowing, ΔC_L = -0.11, is reduced in comparison to the α = 0° case. The change in lift coefficient for the upstream blowing jet is ΔC_L = - 0.18. At α = 8°, the baseline case exhibits flow separation near the trailing-edge. As a result, the camber effect is diminished for normal blowing as the change in lift coefficient reduces to ΔC_L = - 0.09, whereas there is still some effect with the upstream blowing.

Flow separation initiates near the leading edge of the airfoil for all cases investigated at α = 13°. The width of the separated region changes little with normal blowing, whereas there is a much larger separated region with upstream blowing. The streamlines of the inset figure show that the normal jet creates a weak flow in the downstream direction, eliminating the reverse flow near the surface. In contrast, the direction of the flow near the upstream blowing slot is in the upstream direction. The effect appears to propagate upstream and deflect the separated shear layer further away from the wall. Even a small change in the deflection angle near the leading-edge appears to be significant in terms of lift reduction. The momentum injected tangentially along the surface with upstream blowing modifies the reversed flow in the separated region. This enlarged recirculation zone is in agreement with the force measurements observed in Fig. 5c. This is consistent with the observations of Kearney and Glezer [25], who demonstrated that bleed near the leading-edge can provide substantial lift reduction near the stall angle by means of subtle changes in the separation angle of the shear layer. In our case this is achieved with upstream blowing from near the trailing-edge in an already separated flow at the stall angle.

In summary, at zero angle of attack, there is not much difference between the two types of blowing at x/c=0.95. We think this is because the mechanism is related to flow deflection at the trailing-edge and the modification of the Kutta condition. In addition, the external flow is close to the surface in the baseline case, unlike increasing distance of the shear layer from the surface with separation at higher angles of attack. Both types of blowing seem effective. In contrast, at α=13°,

the mechanism is related to the modification of the recirculation region. Upstream blowing is capable of deflecting the shear layer further away by penetrating further upstream whereas the normal jet is ineffective. For a given blowing strength, the upstream blowing appears to be more effective than the normal jet. In general, this is due to the ability of the upstream blowing to induce flow separation more effectively. Only near the trailing-edge, the difference between the two is smaller. Upstream blowing jet not only penetrates further upstream, but also generates larger separation zone. The latter effect is documented and predicted in References [10] and [11] for the flat-plate models. Compared to normal blowing (jets in crossflow), upstream blowing (counter flowing wall jets) provide nearly one order of magnitude larger deflection of the freestream flow for the same jet velocity ratio in the range of 1 to 2 according to these studies.

There is an interesting similarity with the observations of flaps (with a length of 12% to 22% of the chord length) placed on the upper surface of an airfoil at stall and post-stall angles of attack [26]. For large flap angles, the flap may deflect the separated shear layer further away, causing a lift reduction. In contrast, for small flap angles for which the flap remains inside the reverse flow region, the flap blocks and decreases the reverse flow from the trailing-edge to the leading-edge, causing a lift increase. Hence, the characteristics of the reverse flow appear to have significant influence on the lift generated in the separated flows. In our case, due to the greater effectiveness of upstream blowing across the board, it was investigated in detail as discussed below.

C. Effect of Flow Rate Coefficient

Figure 7 shows the time-averaged force measurements for upstream blowing for three chordwise locations at all flow rate coefficients considered. Presented in the left column are lift coefficient curves for each jet location; the right column presents the change in lift coefficient relative to the baseline airfoil. When placing the upstream blowing at x_J/c = 0.08 (Figure 7a), the effect of increasing flow rate becomes greater with increasing angle of attack, and reaches maximum around α = 11° just before the stall angle of the baseline airfoil. With increasing flow rate coefficient, the gradient of the lift curve decreases as the point of stall becomes less distinct. Interestingly, stall is brought forward to α = 11° with C_Q = 0.20%, but is delayed to α = 19° with C_Q = 0.44%. The curves converge at α = 13°, where negligible difference between flow rate coefficients is observed. Even the lowest flow rate coefficient is sufficient to induce a lift reduction, i.e., ΔC_L = - 0.28 at α = 13°.

Figure 7b shows a distinct relationship between change in lift coefficient and flow rate coefficient for x_J/c = 0.60, indicating there is a significant benefit to increasing the flow rate for angles below α = 14°. Lift reduction caused by the C_Q = 0.20% jet is relatively insignificant until $\alpha \geq 9°$. The largest lift reduction for this flow rate is noticed at α = 14°, where the peak lift coefficient is diminished by ΔC_L = -0.18 with C_Q = 0.20%. In comparison, the lift coefficient reduction for this angle of attack is ΔC_L = -0.29 for C_Q = 0.44%. Similar to the jet at x_J/c = 0.08, the stall angle is delayed with the maximum flow rate to α = 19°. However, the change between each lift curve appears to reduce with increasing flow rate coefficient, which implies a saturation effect.

Figure 7c shows the time-averaged force measurements for the upstream jet configuration at x_J/c = 0.95. For this location flow rate has greatest effect at lower angles of attack. Upstream blowing with C_Q = 0.20% at α = 5°, causes a decrease in lift by ΔC_L = - 0.11. In comparison, the lift reduction could be increased to ΔC_L = - 0.18 through C_Q = 0.44%. Increasing the flow rate coefficient modifies the lift at zero angle of attack and increases the gradient of the lift curve so that the curves converge at around α = 13°. Blowing at C_Q = 0.40% provides the most consistent lift reduction in the range of ΔC_L = 0.17 – 0.20 up to α = 13°.

Returning to the case of x_J/c = 0.60, Figure 8 presents the time-averaged velocity magnitude fields of the baseline cases and upstream blowing with three different flow rate coefficients. In all PIV plots, the location of the jet is indicated by a short thick line inside the airfoil. Even at zero angle of attack, the effect of increasing flow rate on the separated flow induced by the upstream blowing is evident. However, as shown in Figure 7b, the change in the lift coefficient is relatively small. With increasing angle of attack, the effect of increasing flow rate becomes stronger. The separated shear layer moves away from the surface and the size of the wake increases with increasing flow rate coefficient. This is particularly visible at α = 8° for which the freestream flow is deflected further from the upper surface with increasing flow rate, hence decreasing the effective camber of the airfoil to enhance the lift reduction. Figure 9 presents the respective coefficient of pressure plots for upstream blowing at α = 8°. Despite increasing flow rate, the adverse pressure gradient on the upper surface remains similar. Consequently, suction is reduced upstream of the jet at x_J/c = 0.60, then aft of the jet negative pressure is recovered. The pressure created downstream of the C_Q = 0.20% jet is the same as the baseline case. However, negative pressure in

this region is augmented for the two higher flow rates, C_Q = 0.35% & 0.44%. Upstream blowing with C_Q = 0.35% creates a lift coefficient reduction of 12.2% relative to the baseline case, however this can be enhanced to 16.6% with a flow rate coefficient of C_Q = 0.44%.

As shown in Figure 7b, for x_J/c = 0.60, the effect of flow rate on lift reduction is significant at the stall angle α = 13°. Figure 8 reveals the changes in the size of the circulation region by the upstream blowing. The deflection of the separated shear layer away from the surface of the airfoil is visible. This is surprising given that the jet is submerged completely in the separated region but the effect is clear.

D. Effect of Blowing Location

To directly compare the effect of blowing location, Figure 10 shows the time-averaged lift coefficient and also the change in the lift coefficient with respect to the baseline case for all five chordwise locations for the maximum flow rate coefficient. As noted earlier, trailing edge locations are preferable at low angles of attack. For angles of attack below α = 5°, ΔC_L decreases as the upstream jet location is moved from the trailing edge to the leading edge. For example for α = 0° the change in lift coefficient reduces from ΔC_L = - 0.20 for x_J/c = 0.95 to ΔC_L = - 0.01 for x_J/c = 0.08.

With increasing angle of attack, the lift curve gradient is maintained for blowing locations near the trailing-edge. In contrast, there is significant decrease in the lift curve slope for blowing locations near the leading-edge. As a result, a point of intersection occurs between α = 9° and 11°, where all chordwise locations provide similar lift force. The smaller gradient for blowing near the leading edge means the ability to mitigate lift is enhanced at higher angles of attack. Consequently, the jet at x_J/c = 0.95 creates the smallest reduction in lift at α = 13°. Furthermore, upstream blowing at all chordwise locations extends its influence beyond the stall angle maintaining the lift reduction, even into the post-stall regime.

Time-averaged velocity magnitude and pressure coefficient plots for the maximum flow rate coefficient of C_Q = 0.44% for the baseline case and jet locations x_J/c = 0.08, 0.60 and 0.95 are presented in Figures 11 and 12, respectively. Upstream blowing induces different behavior at different locations. For α = 0°, the effect of upstream blowing is most visible for x_J/c = 0.60 in Figure 11. The effect can be seen in the variation of the pressure coefficient in Figure 12a. The

pressure becomes positive upstream of the blowing location, but then drops to negative values downstream of the blowing location. In contrast, the blowing at x_J/c = 0.08 does not appear to induce separation as shown in Figure 11. Downstream of the jet, the pressure along the upper surface is increased, but is also increased on the lower surface (see Figure 12a). This indicates positioning the jet towards the leading edge influences the lower surface pressure. In contrast, for the jet at x_J/c = 0.95 no acceleration in flow near the jet is observed. However, as indicated by the streamline deflection, the airfoil experiences an effective decrease in camber towards the trailing edge creating an upwash effect, and therefore effective lift mitigation. Pressure along the entire upper surface is increased which ultimately causes the reduction in lift.

As the angle of attack increases to α = 5°, for x_J/c = 0.08, a separation bubble (in the time-averaged sense) extending to $x/c \approx 0.30$ seems to exist. Streamlines indicate a slight deflection in flow path due to this short separation bubble. Ahead of the jet location, the region of high velocity magnitude reduces significantly. Acceleration of flow near x/c = 0.08 induces greater suction in the region $0.08 \leq x/c \leq 0.20$ (see Figure 12b). The point of maximum suction has moved from x/c = 0.01 for the baseline case to x/c = 0.10 for jet at x_J/c = 0.08, with peak suction increasing from $C_{(p,min)}$ = - 0.91 to $C_{(p,min)}$ = - 1.30. However, downstream of x/c = 0.20 suction is similar to that of the baseline case, explaining the marginal loss in lift, ΔC_L = -0.07. This behavior is also observed for x_J/c = 0.60, except the separation extends beyond the trailing edge. We note that the x_J/c = 0.95 case still creates greater lift reduction, ΔC_L = -0.18 versus ΔC_L = -0.09.

At α = 8°, the airfoil is approaching the region in which all three jet positions create similar lift mitigation (see Figure 10), their behavior is however very different. For x_J/c = 0.08, blowing causes a large recirculation region as seen in Figure 11. One would expect the large separated region created by the jet at x_J/c = 0.08 would incite a greater change in lift in comparison to the jet at x_J/c = 0.95. However, while a suction loss ahead of the jet at x_J/c = 0.08 is visible in Figure 12, the pressure created beyond x/c = 0.10 is similar to that of the baseline case. In contrast, the jet at x_J/c = 0.95 influences the pressure along the entire upper surface, thereby explaining the alleviation in lift of ΔC_L = -0.17. For x_J/c = 0.60, the jet exhibits behavior similar to α = 5°, with the separated region slightly enlarged. Although velocity flow fields indicate significant differences in performance for the jets at x_J/c = 0.08, 0.60 and 0.95, the three cases produce similar lift mitigation by $\Delta C_L \approx$ -0.11 to -0.17 with x_J/c = 0.95 still the most effective.

At α = 13°, for x_J/c = 0.08 the shear layer is displaced upwards at a greater angle producing a larger wake region, as seen in Figure 11. The shear layer deflection and larger separated region is fundamental to the increased lift alleviation of ΔC_L = -0.33. The upper surface pressure increases significantly (less suction) due to the separation and the suction peak at *x/c* = 0.01 diminishes, see Fig. 12d. In addition, the lower surface experiences a decrease in pressure. It follows that, positioning the jet closer to the leading edge has a greater effect on lower surface. Jet at x_J/c = 0.60 and x_J/c = 0.95 produces similar flow fields. The ability of upstream blowing to manipulate the flow separation near the leading-edge for x_J/c = 0.60 and x_J/c = 0.95 is remarkable. Nevertheless, blowing near the leading-edge is more effective.

In summary, the location of the jet as well as the angle of attack are the most important parameters. The magnitude of the adverse pressure gradient in the baseline case is relatively small at low angles of attack, therefore it is more difficult to force the flow to separate or there might be reattachment (see for example α=0° and 5°, when the jet is located at *x/c* = 0.08. Hence, lift reduction is ineffective. In contrast, at higher angles of attack, the magnitude of the adverse pressure gradient becomes larger and it becomes easier to separate the flow for the same jet location. As a result, optimal location of blowing moves upstream with increasing angle of attack.

IV. Conclusions

Force, pressure and two-dimensional PIV measurements were performed for counter flowing wall jets placed on the upper surface of a NACA0012 airfoil and their effectiveness for lift reduction was compared with that of normal blowing. Upstream blowing is more effective than normal blowing for the same flow rate coefficient or the same momentum coefficient. The main advantage of upstream blowing over normal blowing was found at higher angle of attack near stall. Even for completely separated flows, upstream blowing near the trailing-edge can modify the recirculation region and deflect the separated shear layer upwards. This subtle change causes significant lift reduction and represents a clear advantage over mechanical devices (mini flaps) placed near the trailing-edge, which remain ineffective in the separated flows.

There are two contrasting mechanisms for lift reduction. These are the conventional method of flow deflection and effective camber, which is more effective at low angles of attack and near the trailing edge; and forced separation, which is more effective at high angles of attack and near the leading edge. The effect of increasing flow rate coefficient on the magnitude of lift reduction

depends on the angle of attack and blowing location. The largest effect of blowing location is found at zero angle of attack with a peak reduction of ΔC_L = -0.22. Blowing near the trailing-edge is preferable at low angles of attack. The effect of blowing location diminishes with increasing angle of attack, but then amplifies again near the stall angle. Blowing near the leading-edge is preferable at the stall angle of attack, where a maximum lift reduction of ΔC_L = -0.33 was observed. Largest deflection of the separated shear layer is achieved with upstream blowing near the leading-edge. The next step of the investigation is the unsteady response of the lift force to the transient actuation of counter-flowing jets, which will be the subject of a second paper.

Acknowledgments

The authors would like to acknowledge the support from the EPSRC studentship, Airbus UK, the EPSRC strategic equipment grant (EP/K040391/1 & EP/M000559/1) and EPSRC project (EP/M022307/1).

References

[1] Xu, J. and Kroo, I. "Aircraft Design with Active Load Alleviation and Natural Laminar Flow", *Journal of Aircraft,* vol. 541, no. 5, 2014, pp. 1532-1545.

[2] Moulin, B., Karpel, M., "Gust Loads Alleviation Using Special Control Surfaces", *Journal of Aircraft,* Vol. 44, No. 1, 2007, pp. 17-25.

[3] Heinz, J., Sørenson, N. N., Zahle, F., "Investigation of the Load Reduction Potential of Two Trailing Edge Flap Controls Using CFD", *Wind Energy*, Vol. 14, No, 3, 2011, pp. 449-462.

[4] Blaylock, M., Chow, R., Cooperman, A., and van Dam, C. P., "Comparison of Pneumatic Jets and Tabs for Active Aerodynamic Load Control," *Wind Energy Journal,* Vol. 17, No. 9, 2014, pp. 1365-1384.

[5] Heathcote, D. J., Cleaver, D. J., Gursul, I., "Aerodynamic Load Alleviation Using Mini-tabs", *Journal of Aircraft,* under review. See also, "An Experimental Study of Mini-Tabs for Aerodynamic Load Control", *54th AIAA Aerospace Sciences Meeting*, AIAA Paper 2016-0325, 2016, pp. 1-22.

[6] Boeije, C. S., de Vries, H., Cleine, I., van Emden, E., Zwart, G. G. M., Stobbe, H., Hirschberg, A., and Hoeijmakers, H. W. M., "Fluidic Load Control for Wind Turbine Blades," 47th *AIAA Aerospace Sciences Meeting Including The New Horizons Forum and Aerospace Exposition*, AIAA Paper 2009-684, 2008, pp. 1-8.

[7] Spence, D. A., "The Lift Coefficient of a Thin, Jet-Flapped Wing," *Proceedings of the Royal Society of London. Series A, Mathematical and Physical Sciences*, Vol. 238, No, 1212, Dec. 1956, pp. 46-68.

[8] Traub, L. W., Miller, A. C., and Rediniotis, O., "Comparisons of a Gurney and Jet Flap for Hingeless Control," *Journal of Aircraft*, Vol. 41, No. 2, 2004, pp. 420-423.

[9] Mahesh, K., "The Interaction of Jets with Crossflow", *Annual Review of Fluid Mechanics,* vol. 45, 2013, pp. 379-407.

[10] Balachandar, R., Robillard, L. and Ramamurthy, A.S., "Some Characteristics of Counter Flowing Wall Jets", *Journal of Fluids Engineering Transactions of the ASME,* vol. 114, 1992, pp. 554-558.

[11] Hopkins, D.F. and Robertson, J.M., "Two-Dimensional Incompressible Fluid Jet Penetration", *Journal of Fluid Mechanics,* vol. 29, 1967, pp. 273-287.

[12] Feng, L.H., Choi, K.S., Wang, J.J., "Flow Control over an Airfoil Using Virtual Gurney Flaps", *Journal of Fluid Mechanics,* vol. 767, 2015, pp. 595-626.

[13] Barlow, J. B., Rae, W. H., Jr., and Pope, A., *Low-Speed Wind Tunnel Testing*, 3rd ed., John Wiley & Sons, Inc., New York, 1999, pp. 309.

[14] Chen, C., Seele, R., and Wygnanski, I., "Flow Control on a Thick Airfoil Using Suction Compared to Blowing", *AIAA Journal*, vol. 51, 2013, pp. 1462-1472.

[15] Wang, Z. and Gursul, I., "Lift Enhancement of a Flat-Plate Airfoil by Steady Suction", *AIAA Journal*, vol. 55, 2017, pp. 1355-1372.

[16] Jones, R., Cleaver, D. J., Gursul, I., "Aerodynamics of Biplane and Tandem Wings at Low Reynolds Numbers", *Experiments in Fluids,* Vol. 56, No. 6, 2015, pp.1-25.

[17] Cleaver, D. J., Wang, Z., Gursul, I., Visbal, M. R., "Lift Enhancement by Means of Small-Amplitude Airfoil Oscillations at Low Reynolds Numbers", *AIAA Journal*, Vol. 49, No. 9, 2011, pp. 2018-2033.

[18] Moffat, R. J., "Describing the Uncertainties in Experimental Results", *Experimental Thermal and Fluid Science,* Vol. 1, No. 1, 1988, pp. 3-17.

[19] Prasad, A. K., "Particle Image Velocimetry" , *Current Science,* Vol. 79, No. 1, 2000, pp. 51-60.

[20] Sheldahl, R. E., and Kilmas, P. C., "Aerodynamic Characteristics of Seven Symmetrical Airfoil Sections Through 180-Degree Angle of Attack for use in Aerodynamic Analysis of Vertical Axis Wind Turbines," Sandia National Laboratories SAND80-2114, Mar. 1981.

[21] Jacobs. E. N., and Sherman, A., "Airfoil Section Characteristics as Affected by Variations of the Reynolds Number," NACA Report 586, 1937, pp. 227-267.

[22] Lockwood, V.E. and Vogler, R.D., "Exploratory Wind Tunnel Investigation at High Subsonic and Transonic Speeds of Jet Flaps on Unswept Rectangular Wings", NACA Technical Note 4353, August 1958.

[23] Dimmock, N.A., "Some Further Jet Flap Experiments", Aeronautical Research Council Technical Report, C.P. No. 345, 1957.

[24] Cooperman, A. M., "Wind Tunnel Testing of Microtabs and Microjets for Active Load Control of Wind Turbine Blades," Ph.D. Dissertation, Mechanical and Aeronautical Engineering Dept., University of California, Davis, 2005.

[25] Kearney, J.M. and Glezer, A., "Aero-Effected Flight Control Using Distributed Active Bleed", *AIAA-2011-3099,* AIAA Conference, 2011, Hawaii.

[26] Meyer, R., Hage, W., Bechert, D.W., Schatz, M., Knacke, T. and Thiele, F., "Separation Control by Self-Activated Movable Flaps", *AIAA Journal,* vol. 45, 2007, pp. 191-199.

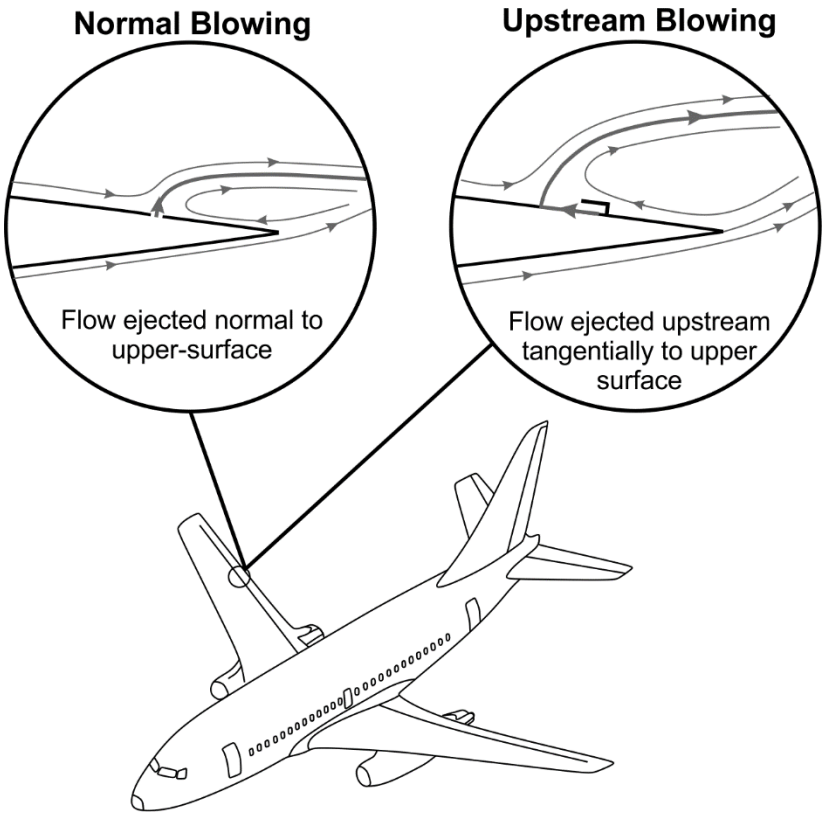

Figure 1. Load control concepts.

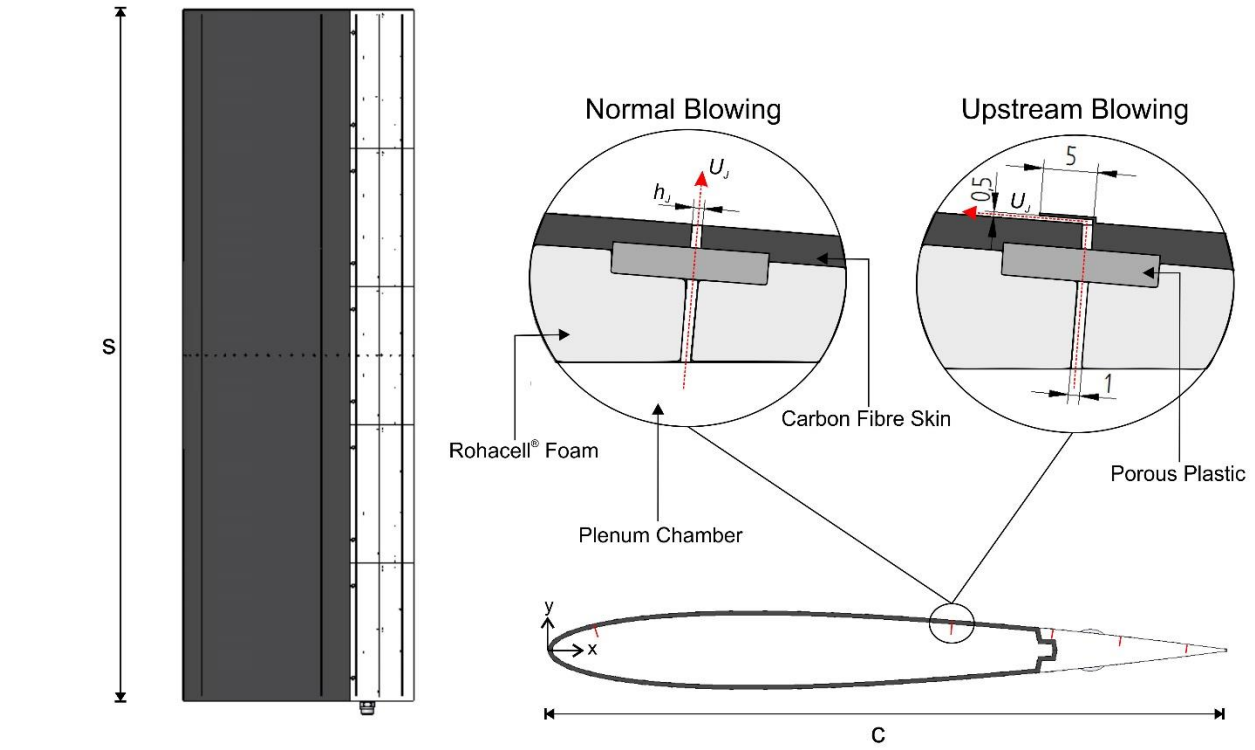

a)

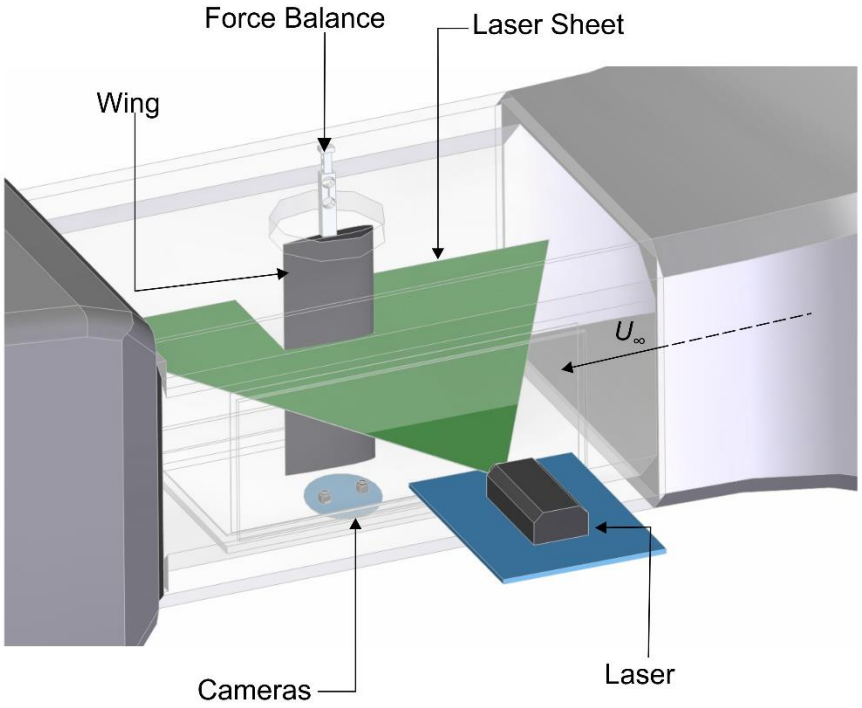

b)

Figure 2. a) Wing design and chordwise locations of jets, dimensions in millimeters; b) Experimental setup.

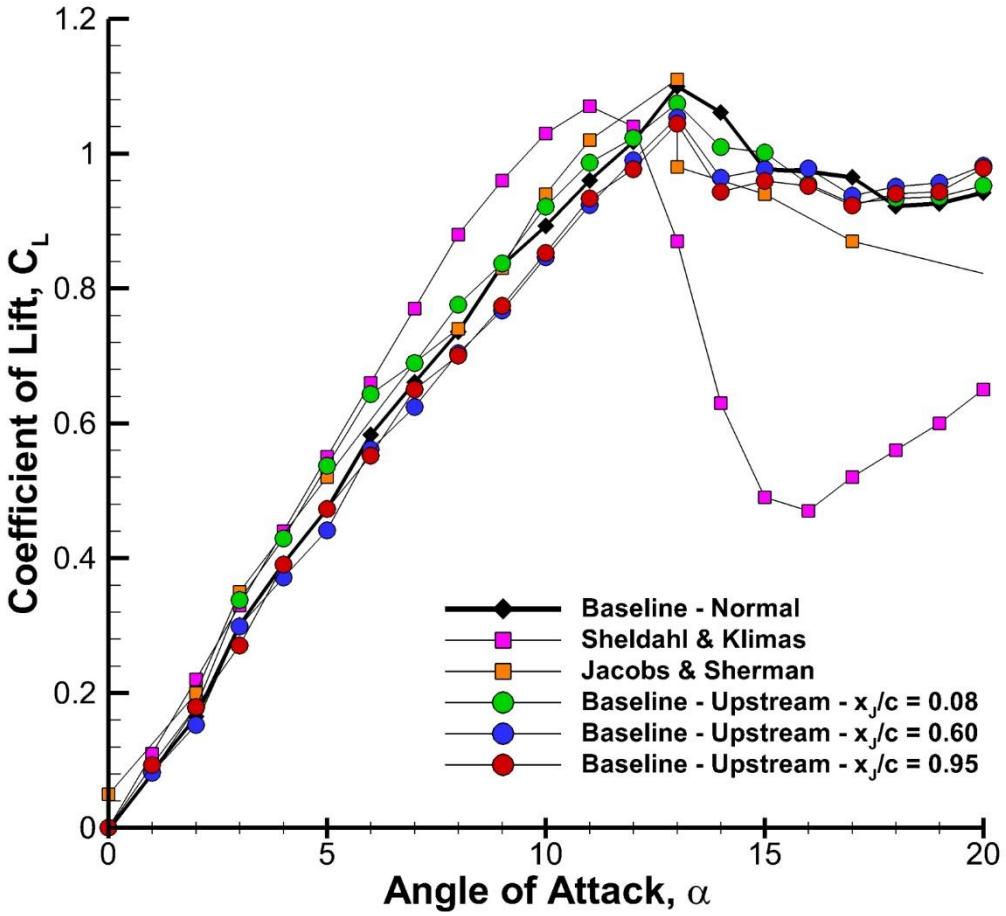

Figure 3. Baseline measurements for the NACA0012 airfoil.

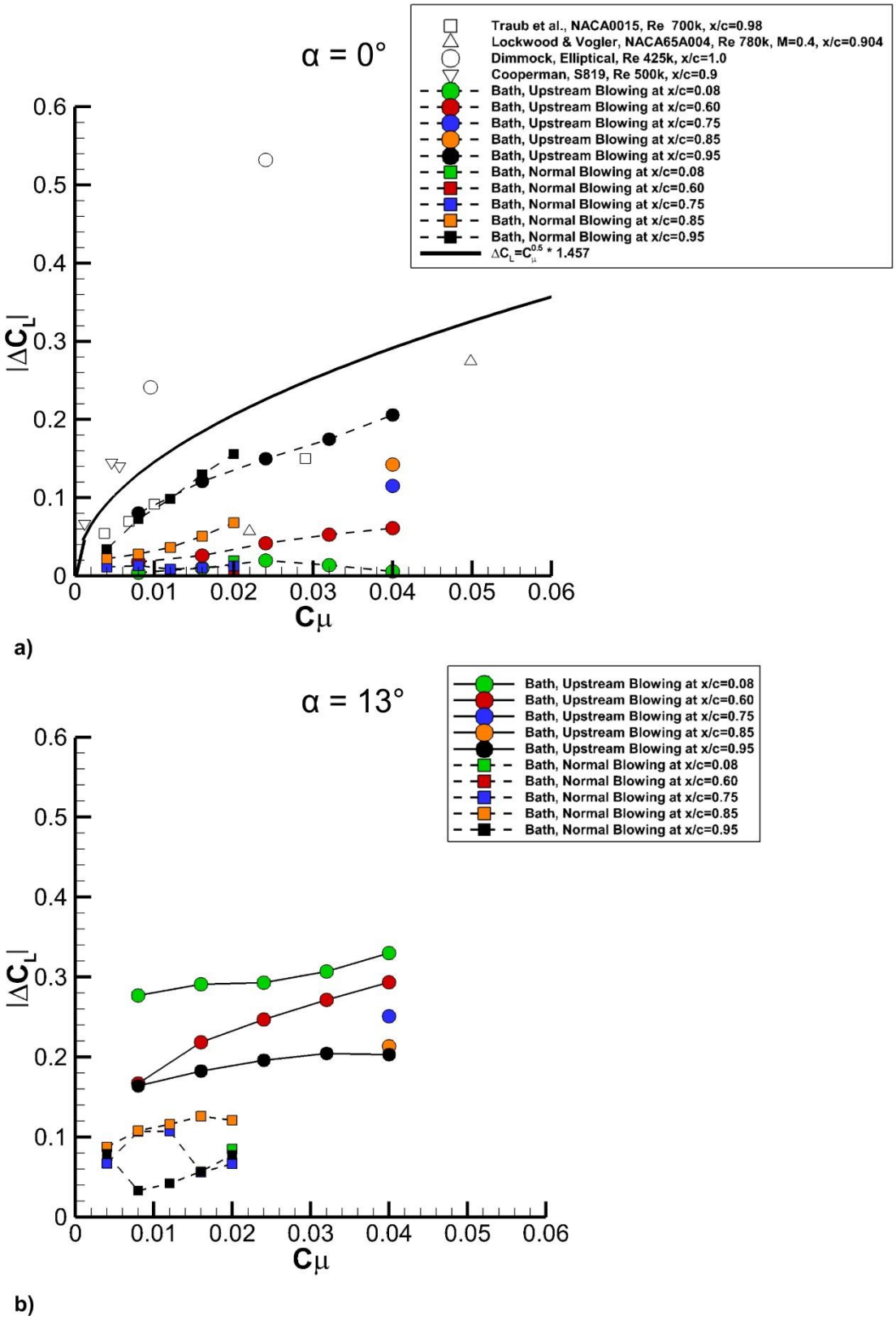

Figure 4. Change in lift coefficient as a function of momentum coefficient, for a) α = 0° and b) α = 13°.

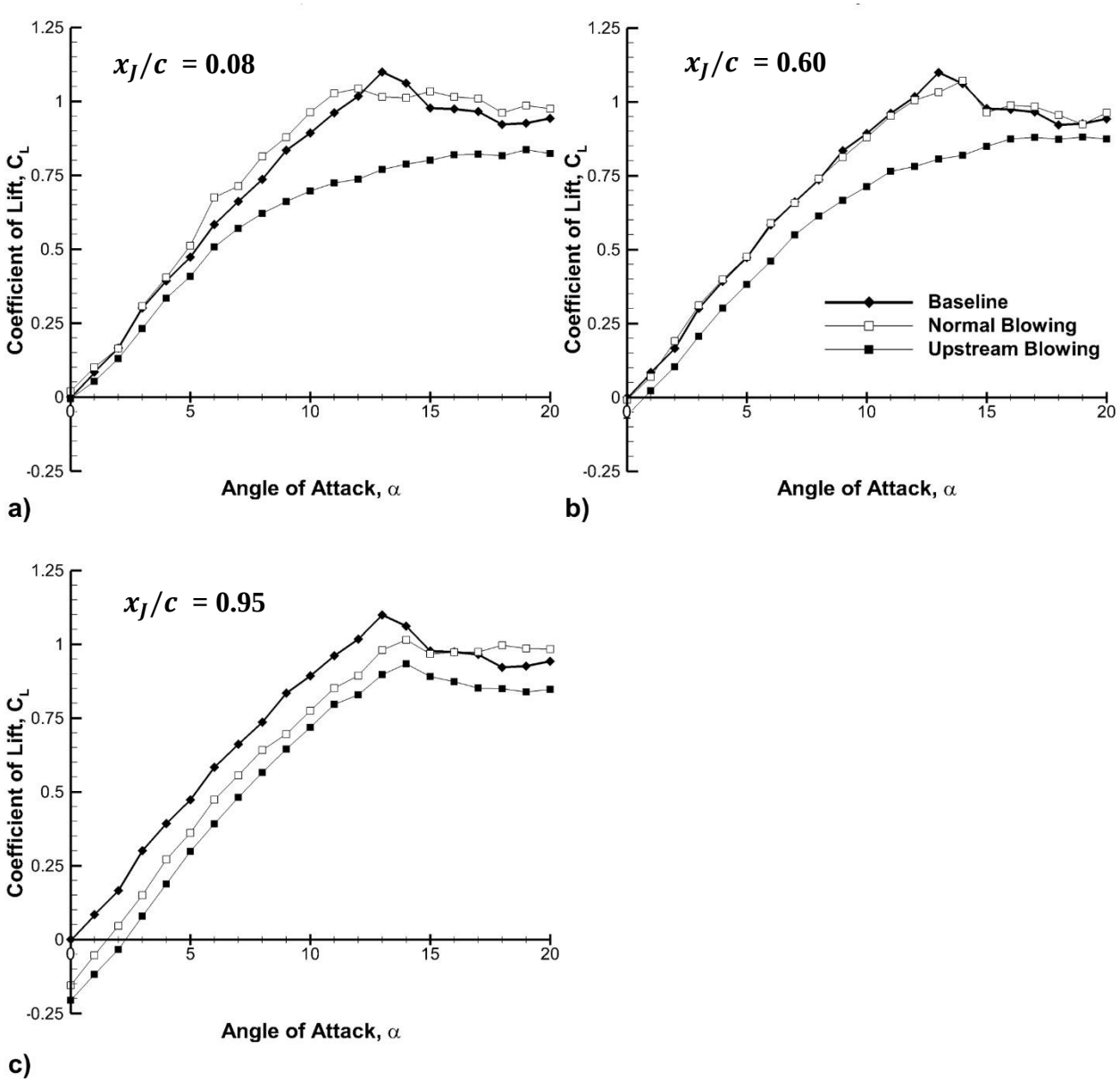

Figure 5. Lift coefficient as a function of angle of attack for normal blowing (C_μ=2.0%) and upstream blowing (C_μ=4.0%), for the same flow rate coefficient of C_Q = 0.44%, for: a) x_J/c = 0.08; b) x_J/c = 0.60; c) x_J/c = 0.95.

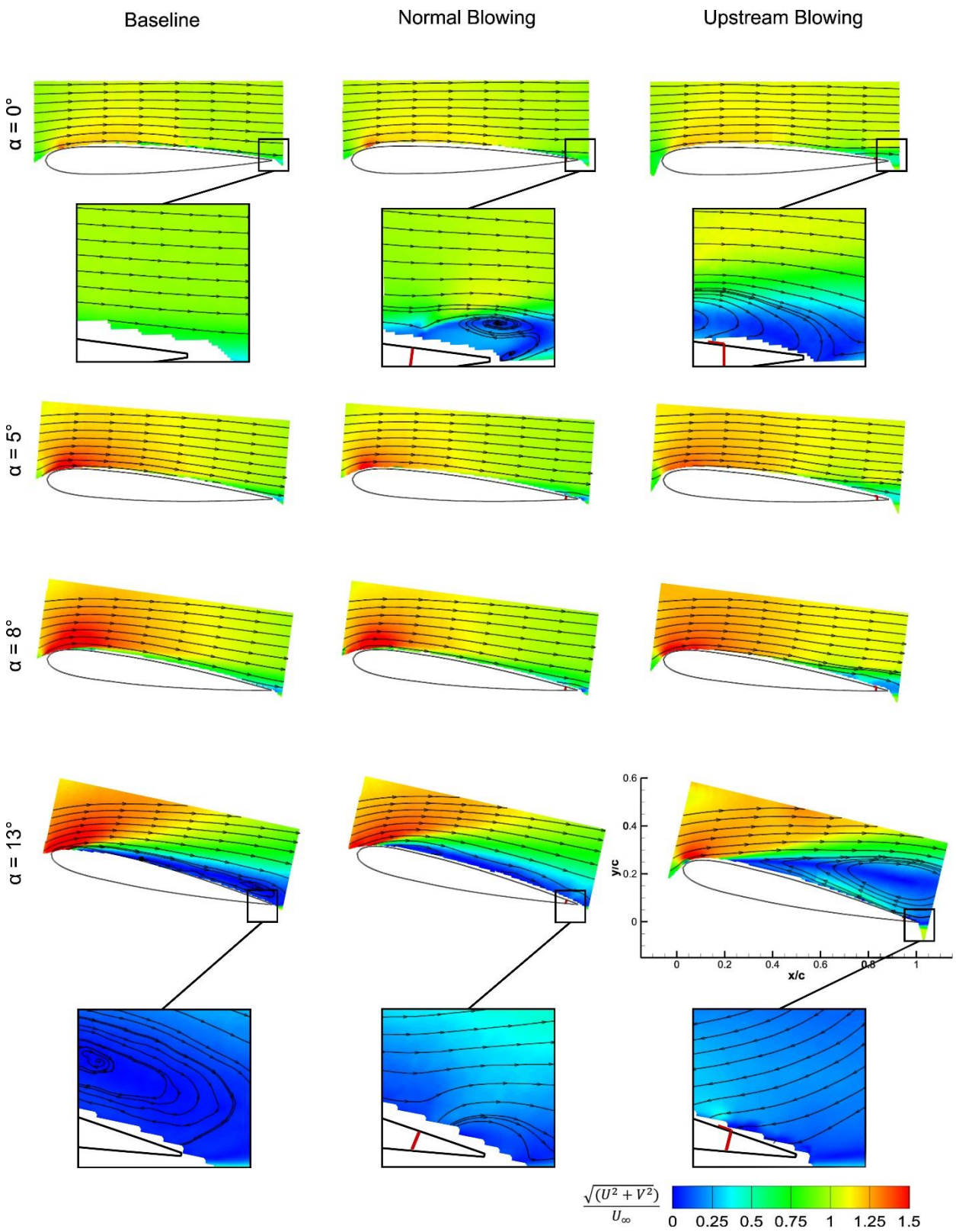

Figure 6. Time-averaged velocity comparing normal blowing (C_μ=2.0%) and upstream blowing (C_μ=4.0%), for the same flow rate coefficient of C_Q = 0.44%, for x_J/c = 0.95 and α = 0°, 5°, 8° & 13°. *Re* = 660,000.

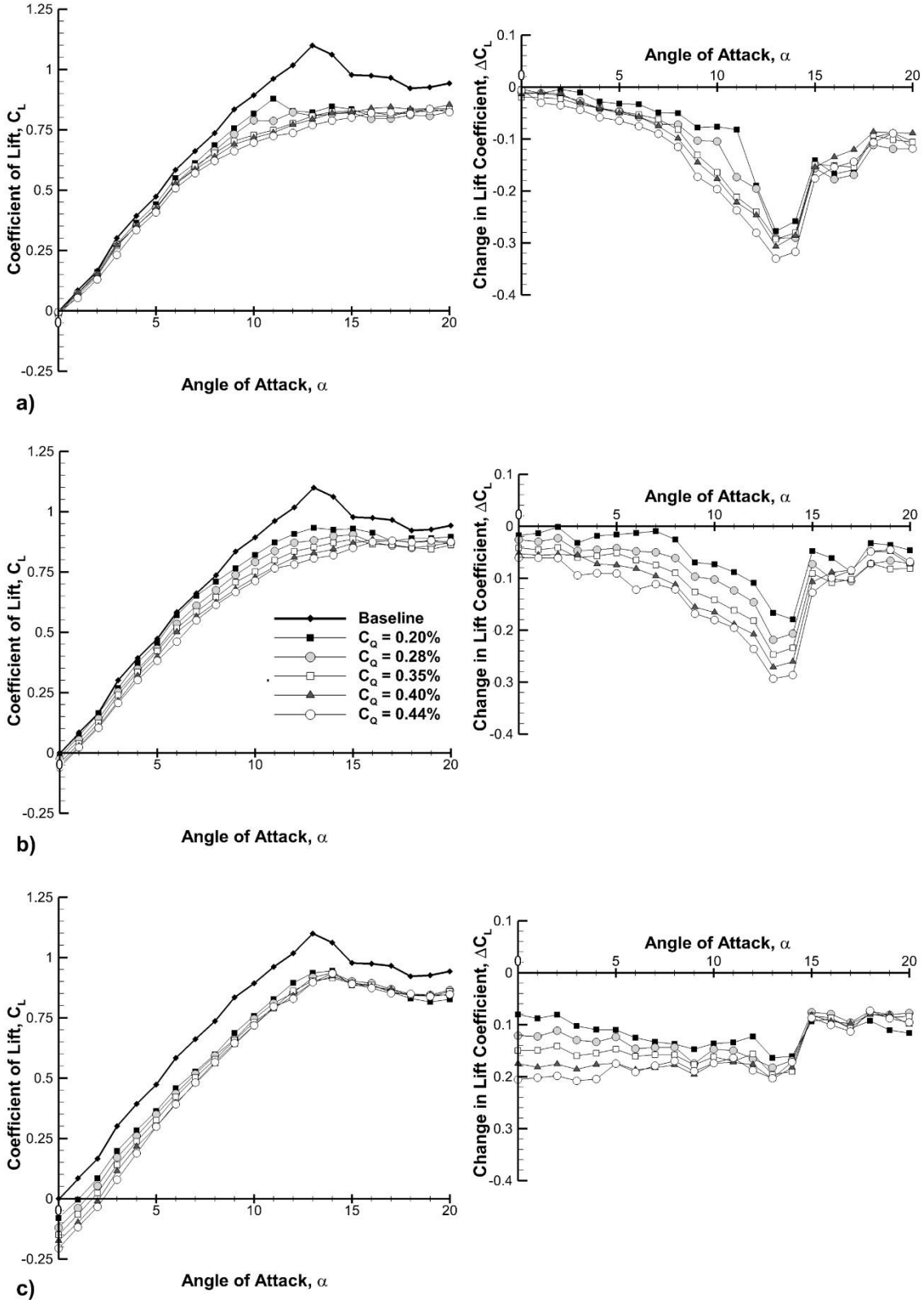

Figure 7. Variation of lift coefficient (left) and change in lift coefficient (right) for upstream blowing, showing the effect of varying flow rate coefficient for a) x_J/c = 0.08; b) x_J/c = 0.60; c) x_J/c = 0.95.

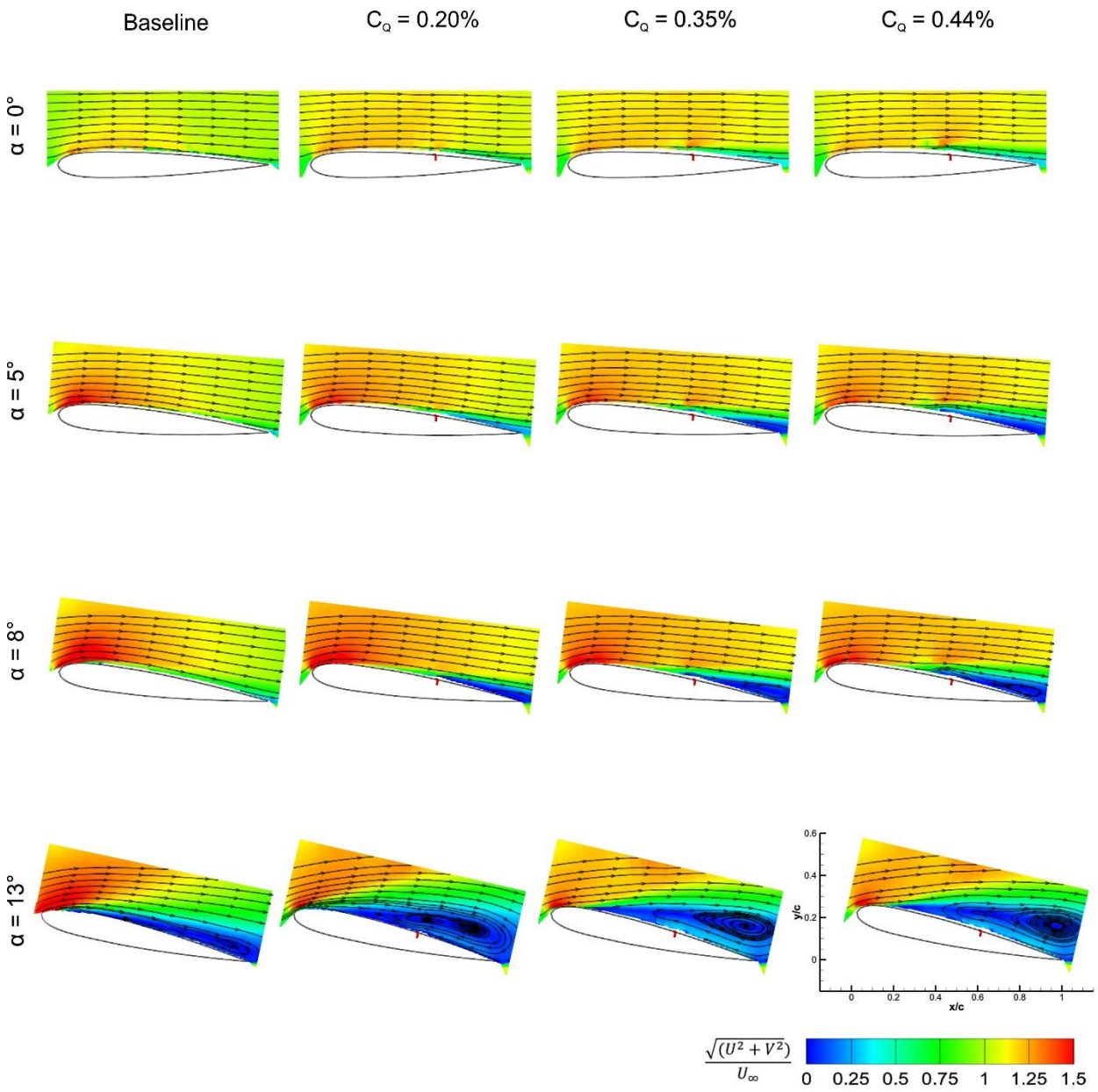

Figure 8. Time-averaged velocity fields for upstream blowing for x_J/c = 0.60, C_Q= 0.20%, 0.35% & 0.44% at α = 0°, 5°, 8° & 13°. *Re* = 660,000.

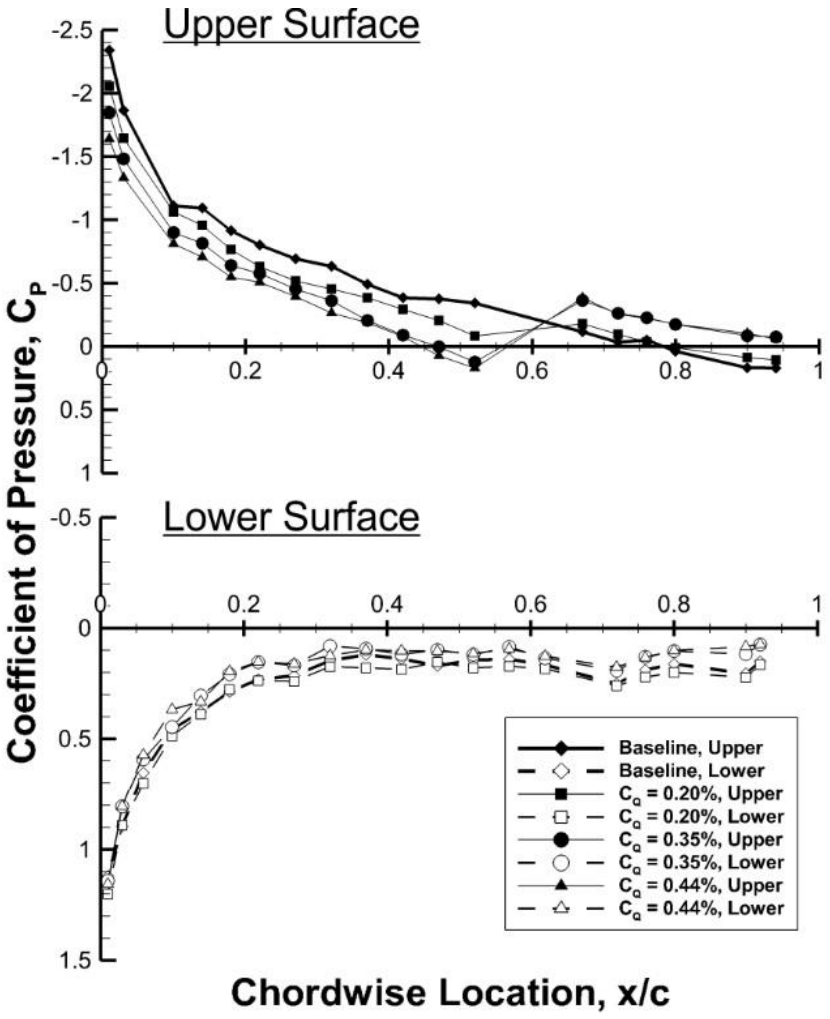

Figure 9. Coefficient of pressure for x_J/c = 0.60, α = 8° for C_Q = 0.20%, 0.35% & 0.44%

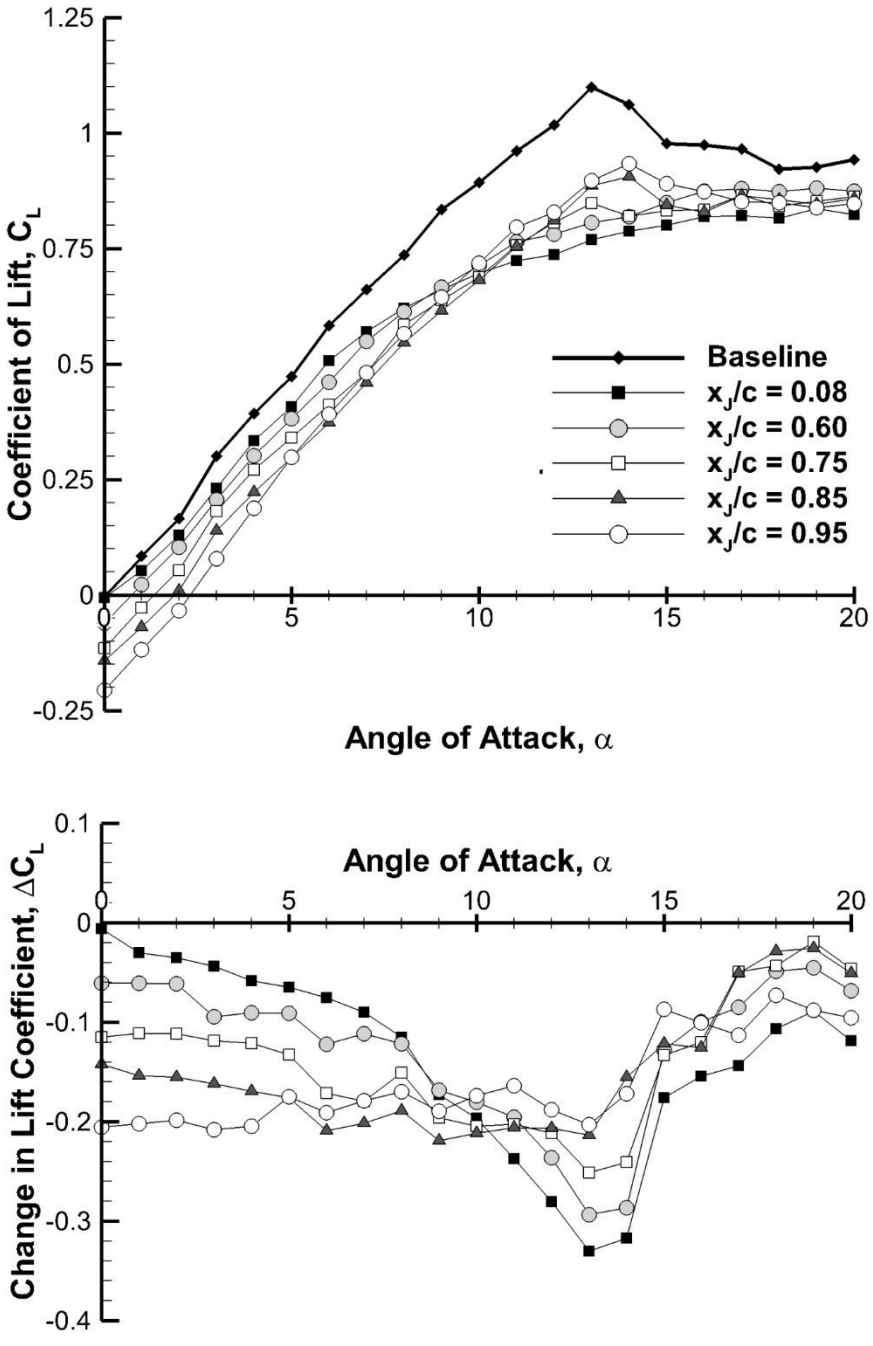

Figure 10. Effect of varying chordwise location of blowing for C_Q = 0.44%.

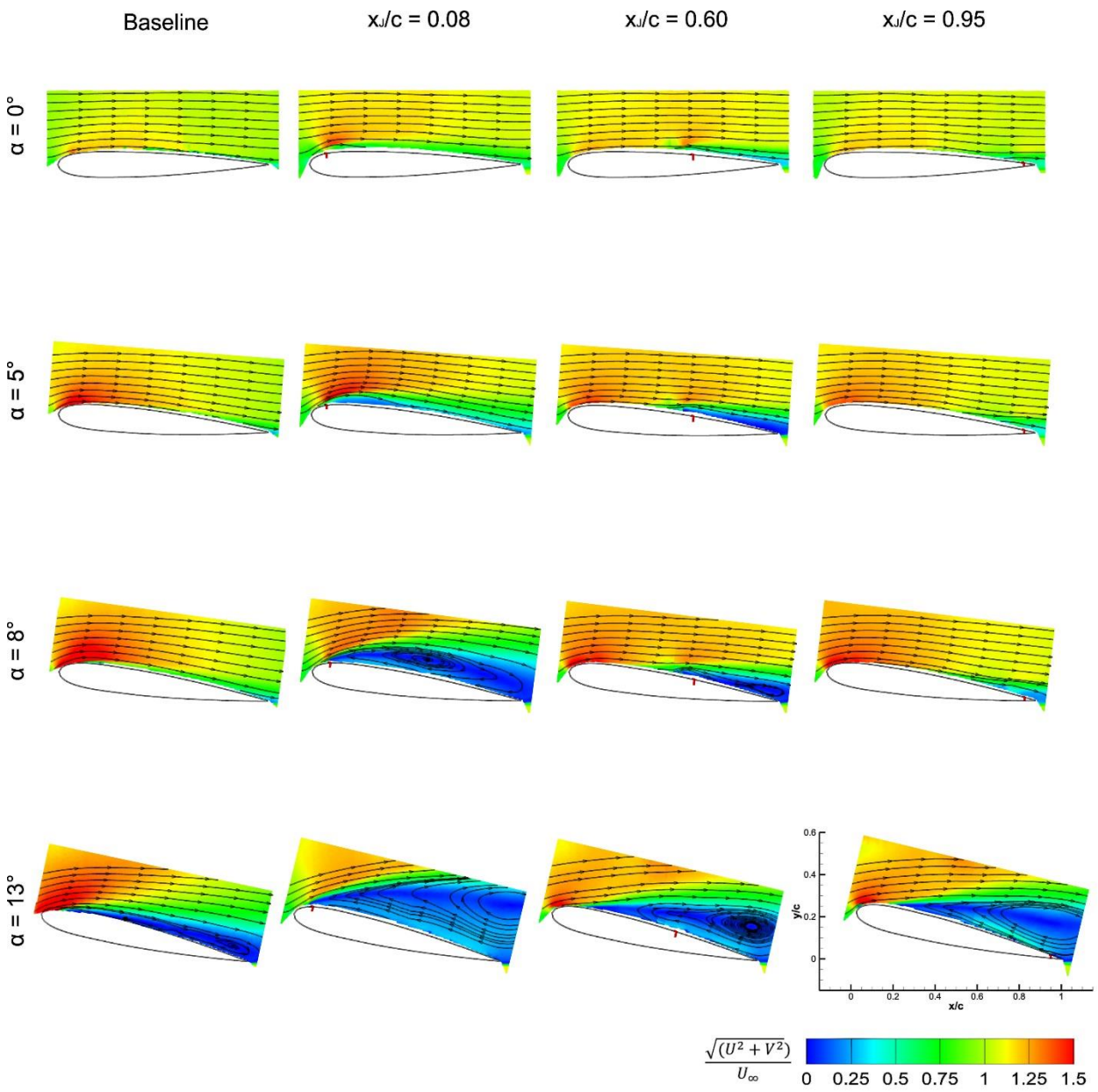

Figure 11. Time-averaged velocity fields for upstream blowing for x_J/c = 0.08, 0.60 & 0.95, C_Q = 0.44% and α = 0°, 5°, 8° & 13°. *Re* = 660,000.

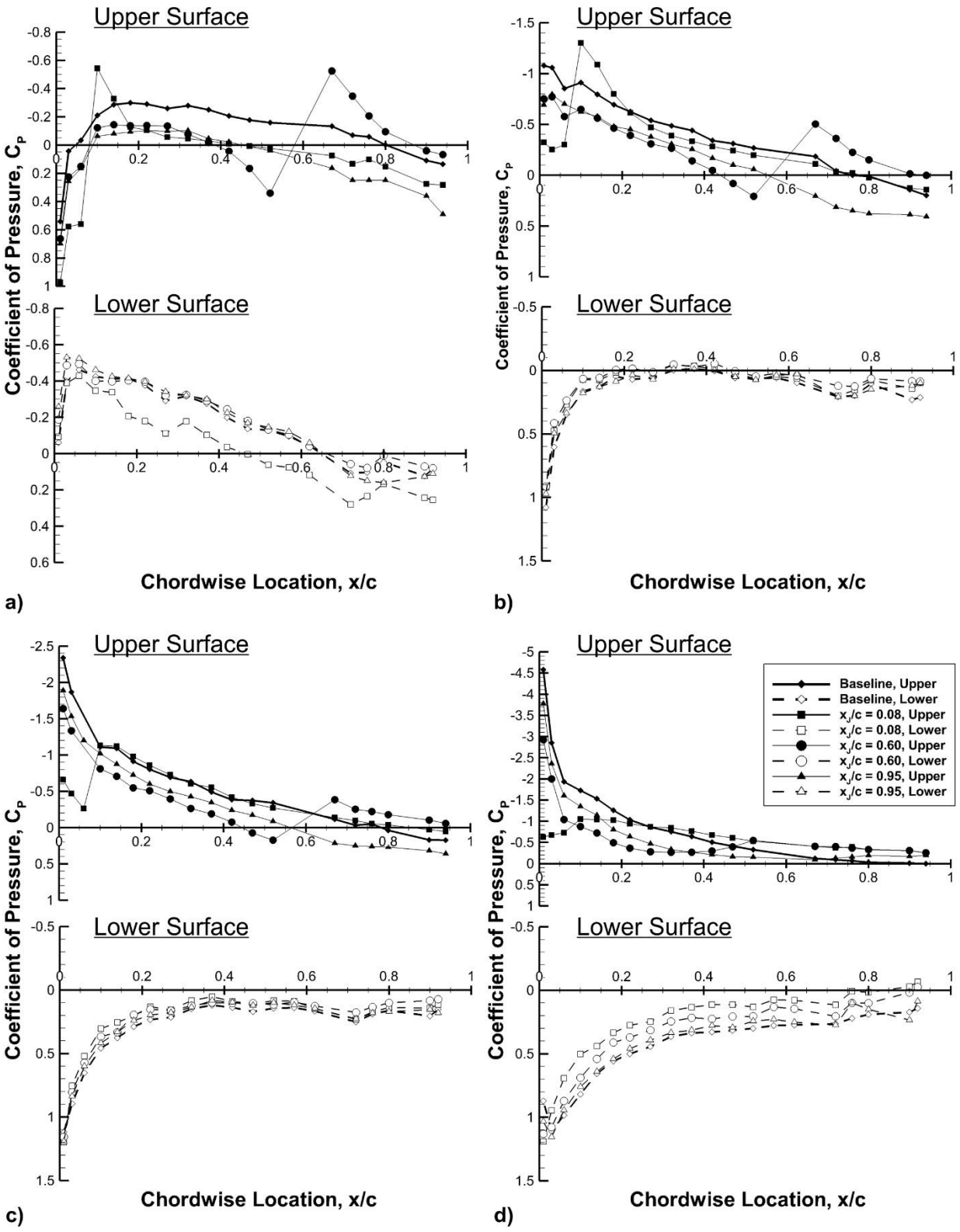

Figure 12. Coefficient of pressure for upstream blowing for x_J/c = 0.08, 0.60 & 0.95, C_Q = 0.44% at: a) α = 0°; b) α = 5°; c) α = 8°; d) α = 13°.